

Research

Series Resistance Imaging in Solar Cells by Lock-in Thermography

O. Breitenstein^{1*}, J. P. Rakotoniaina¹, A. S. H. van der Heide² and J. Carstensen³

¹Max Planck Institute of Microstructure Physics, Weinberg 2, D-06120 Halle, Germany

²Energy Research Centre of the Netherlands ECN, Westerduinweg 3, NL-1755 LE Petten, Netherlands

³Christian-Albrechts-University Kiel, Kaiserstr. 2, D-24143 Kiel, Germany

Two operation modes of lock-in thermography are introduced to detect regions of high series resistance in solar cells. These are differential techniques, working in the dark and under illumination, where images taken under two different conditions are used to calculate an image, which is especially sensitive to series resistance variations. Though the series resistance cannot be measured quantitatively by these techniques, regions of increased emitter contact resistance can be reliably detected. A realistic electrothermal modelling of a series resistance defect in a solar cell with and without illumination is presented. The new thermographic techniques are compared with established techniques for series resistance imaging. Especially the technique working under illumination gives results that agree very well with those of other methods. Copyright © 2005 John Wiley & Sons, Ltd.

KEY WORDS: silicon solar cells; series resistance; lock-in thermography

1. INTRODUCTION

Infrared (IR) lock-in thermography (LIT) has proven to be a powerful tool for analysing energy losses in solar cells.^{1–6} Originally introduced for imaging shunting phenomena by applying a pulsed bias to the investigated cell in the dark,^{1–3} this technique was recently further developed to image power losses under pulsed illumination of the cell.^{4–6} Here the excitation of the cell is performed by pulsed light under a time-constant load condition. The main advantages of using light irradiation are the ability to investigate solar cells in an early technological state before contacts are made, the possibility to image lifetime-induced inhomogeneities of the diffusion current without facing series resistance problems, and generally the investigation of cells under realistic (illuminated) operation conditions. Since this development was performed independently by two different groups, the terms illuminated lock-in thermography (ILT)^{4,5} and light-modulated lock-in thermography (LimoLIT)⁶ both have been proposed for one and the same type of investigation. However, this is not the first attempt to investigate power losses in solar cells thermally under light irradiation. In 1998 Rappich *et al.*⁷

* Correspondence to: O. Breitenstein, Max Planck Institute, Weinberg 2, D-06120 Halle, Germany.

[†]E-mail: breiten@mpi-halle.mpg.de

Contract/grant sponsor: BMBF Germany; contract/grant number: 0329846 D (ASIS).

introduced a technique to image power losses in solar cells by switching a current source in the dark or a load under constant illumination on and off for 10 s each. By subtracting thermograms captured at the end of the on- and off-phases from each other, this 'thermographic sampling technique' was a kind of lock-in thermography working at 0.05 Hz and detecting the -90° image, which is used also now as a quantitative measure of power losses.²⁻⁴ Obviously, a large number of different lock-in thermography experiments can be performed under illumination on solar cells. To avoid further confusion by the invention of new names for similar techniques, and accepting that LIT is the accepted abbreviation for lock-in thermography for many years, herewith we propose to use the general term illuminated lock-in thermography (ILIT) for all LIT techniques working by any kind of illumination of the cell and the term dark lock-in thermography (DLIT) for all LIT investigations performed in the dark. Special prefixes, such as oc-ILIT, mpp-ILIT, mpp-DLIT, or sc-ILIT may indicate whether the investigation has been performed under open-circuit, at maximum power point, or under short-circuit conditions, for example.

The series resistance R_s is the source of one of the dominant power losses in solar cells. Up to now all LIT investigations of series resistance were based on the detection of Joule heating in regions of horizontal current flow in the emitter and have remained qualitative.⁴ Hence, they aimed to show locations of excessive Joule heating, but did not lead to an image that could be interpreted as a series resistance image. Established techniques for imaging the local series resistance are contact resistance scanning (Corescan)^{8,9} and solar CELl local characterization (CELLO).^{10,11} The Corescan technique relies on mechanical probing of the emitter potential of a cell under illumination under short circuit conditions, where regions of high series resistance show a higher emitter potential. This technique is patented¹² and commercially available,¹³ and it has proven to be very successful to image regions of poor emitter contact resistance. The duration of a scan delivering about 50 000–100 000 points is typically 10–20 min, depending on cell size. However, the Corescan technique uses rasping by the mechanical probe to obtain electrical contact to the emitter, thereby penetrating an insulating anti-reflection coating and slightly damaging the emitter and the fingers. Recently, the force exerted to the fingers could be reduced significantly by replacing the vertical probe with a non-vertical one. Although this results in a longer scan duration because it is only possible to scan in the 'pull' direction with this probe, it is beneficial in the case of rather weak fingers by the prevention of finger cutting. The CELLO technique, on the other hand, is a lock-in technique which measures the local laser-modulated light-beam-induced current (LBIC) and the light-beam-induced voltage (LBIV) at various bias conditions along the I - V curve under homogeneous illumination. The information about the series resistance is derived by combining the results of the current response at short-circuit condition and the voltage response of the whole cell at open-circuit, which reacts most sensitively to variations of the series resistance to its laser-illuminated region.^{10,11} Like LIT, this technique is non-destructive, and it can also be used to investigate shunting phenomena. However, shunts below grid lines are not accessible by CELLO, since this is an optical technique, and a high-resolution investigation of one cell (delivering about 452 000 data points) takes up to several hours. Of course, the acquisition time of a CELLO measurement would considerably reduce, if a similar amount of data points as in the Corescan measurement were measured. Such a possibility using a well-defined defocus of the laser beam is presently under development. Presently, Corescan effectively needs about 7 ms and CELLO about 40 ms measurement time per data point. For both techniques work is underway to speed up the measurement.

The fundamental thermal processes in an illuminated solar cell have been briefly described in a recent publication,¹⁴ leading to the suggestion of a thermal technique for series resistance imaging under illumination, called Rs-ILIT. In this contribution this technique will be discussed in more detail, and we extend this modelling to the unilluminated cell and introduce another LIT technique called Rs-DLIT for imaging the series resistance in solar cells in the dark. The physical basis of Rs-DLIT and Rs-ILIT is described in Section 2. A complete electrothermal description of the basic heat dissipation mechanisms in a solar cell in the dark and under illumination is presented. Based on this description, a defect in a solar cell (circular non-contacted region) is modelled, including all thermal processes, and expected Rs-DLIT and Rs-ILIT profiles are modelled. Experimental results of investigations on two different cells suffering from an inhomogeneous emitter contact resistance are introduced in Section 3 and compared with Corescan and CELLO investigations applied to the same cells. These results and the advantages and limitations of the new techniques are discussed in Section 4.

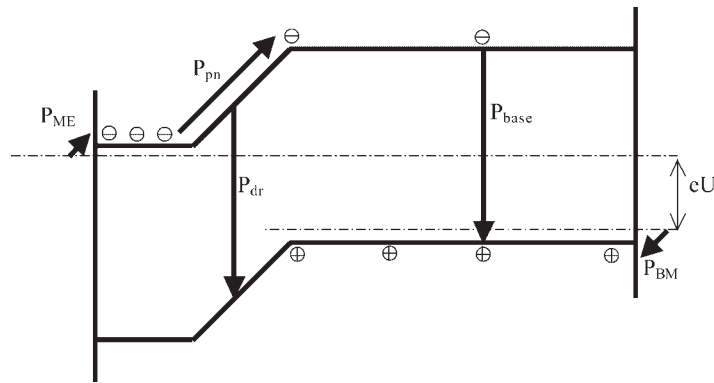


Figure 1. Schematic representation of a pn -junction under forward bias in the dark with the dominant heat sources indicated: Depletion region recombination P_{dr} , base recombination P_{base} , Peltier cooling at the metal-emitter contact P_{ME} , Peltier cooling for electron injection at the pn -junction P_{pn} , Peltier cooling at the base-metal contact P_{BM}

2. PHYSICAL BASIS

Until recently all quantitative interpretations of thermal effects in solar cells were based on the energy conservation law, assuming only heating action, hence for a current I flowing in the dark at a bias U , a heating power of $P = IU$ was expected² to be dissipated in the cell. However, Breitenstein *et al.*³ as well as Kaes *et al.*⁶ have pointed out that Peltier effects may also play a considerable role in solar cells. Hence, if the thermal processes in a solar cell are analysed in detail, they split into different sub-processes, producing either heat (recombination, thermalization) or cooling (Peltier effects), with only the sum of all processes following the energy conservation law. Therefore, based on the earlier analysis,¹⁴ we will start with a detailed discussion of the heat dissipation mechanisms in a solar cell, which goes beyond previous discussions.⁴⁻⁶ In Figure 1 the band diagram of a pn -junction under forward bias in the dark is schematically shown, together with the dominant heat dissipation mechanisms involved. In the following, we are assuming preferential injection of electrons into the base. Hence, we are neglecting hole injection into the emitter. Moreover, radiative carrier recombination is neglected (hence these simulations are realistic only for solar-grade silicon material), and also Joule heating by current flow in the base is neglected. If these processes play a role, corresponding terms can simply be added. In this contribution, the Peltier effect is treated macroscopically for the case of non-degeneracy. Hence, for carriers crossing a junction with a potential step of ΔE , it is assumed that, at a sufficient distance to both sides of a potential step, the free carriers have the same kinetic energy of $3/2 kT$. In this approximation the heating/cooling power generated by a current of I crossing this barrier is $+I - I\Delta E/e$, with the sign depending on the direction of the current. As Figure 1 shows, the dominant heat dissipation mechanisms in the dark are recombination in the depletion region P_{dr} , recombination of injected electrons in the base region or at the back surface P_{base} , Peltier cooling at the metal-emitter contact P_{ME} , Peltier cooling for electron injection at the pn -junction P_{pn} , Peltier cooling at the base-metal contact P_{BM} , and Joule heating due to horizontal current flow in the emitter or in a contact line P_J , not indicated in Figure 1, since this is a local contribution. The contribution P_{pn} comes from the fact that the electrons (and holes for the depletion region recombination current) have to gain the energy of the pn -barrier height before they can be injected into the base or are able to recombine in the depletion region. Without illumination and neglecting ohmic shunting, for a forward current of I and an applied bias of U , the total amounts of these different power contributions are:

$$P_{dr} = \frac{I_{dr}}{e} E_g \quad (1)$$

$$P_{base} = \frac{I_{diff}}{e} E_g \quad (2)$$

$$P_{ME} = \frac{-I}{e} \xi_n \quad (3)$$

$$P_{pn} = \frac{-I}{e} (E_g - \xi_n - \xi_p - eU) \quad (4)$$

$$P_{BM} = \frac{-I}{e} \xi_p \quad (5)$$

$$P_J = \rho_s J_{lat}^2 \quad (6)$$

where I_{dr} = depletion region recombination current, I_{diff} = diffusion (injection) current ($= I - I_{dr}$), e = electron charge, E_g = bandgap energy, ξ_n = difference between Fermi level in n -material to the conduction band edge, ξ_p = difference between Fermi level in p -material to the valence band edge, U = applied forward bias, ρ_s = sheet resistance (in emitter or metallization), J_{lat} = lateral current density (A/m). In the presence of a contact resistance, the power dissipated at the contacts has to be ‘added’ to the contact Peltier cooling. In the presence of ohmic shunting, an extra current contribution bypassing the whole pn -junction has to be added to I .

Assuming homogeneous values for the Fermi energies and that series resistance effects can be neglected (hence if U is constant across the cell), the sum of Equations (1–5) over the whole cell is $P = I U$, as expected from the energy conservation law assuming only heating action. However, all of the processes in Equations (1–6) may be distributed inhomogeneously in a solar cell. For example, local depletion region recombination currents are appear especially at scratches or at the edge region of a solar cell, where the pn -junction reaches the surface, or at positions where other local recombinative defects are crossing the pn -junction. These are the so-called non-linear shunts, which are basically responsible for the ‘second diode’ contribution in the I - V characteristic of silicon solar cells.² From the three possible Peltier contributions, that of the emitter contact is the smallest, since the emitter is highly doped, and that for current injection at the pn -junction P_{pn} is largest. However, except for microscopic investigations, the latter power contribution can not be observed separately, since it is always spatially connected with base recombination heat P_{base} . Any injected carriers recombine typically within a distance of one effective diffusion length from the injection site. Hence, for electron injection into the base always the sum of contributions (Equation 2) and the diffusion part of Equation (4) is locally dissipated, which is:

$$P_{inj} = I_{diff} \left(U + \frac{\xi_n}{e} + \frac{\xi_p}{e} \right) \quad (7)$$

It was mentioned already by Kaes *et al.*⁶ that this amount is larger than $I_{diff}U$. Assuming that all Peltier effects are occurring at the same lateral place as the recombination, hence assuming vertical current flow in the cell, the locally dissipated heat of the diffusion current is $I_{diff} U$, as expected from the energy conservation law based on heating action alone. This will be assumed in the following for our modelling, which considers only vertical current flow in the base and neglects the Peltier effect at the emitter contacts.

If some current flows through the cell, the two-dimensional distribution of the series resistances of the emitter, the contacts, and the grid metallization together with the two-dimensional lateral and vertical current distribution leads to a two-dimensional distribution of the emitter potential $U(x,y)$. The general calculation of $U(x,y)$ from a sheet resistance distribution $\rho_s(x,y)$ in the presence of a pn -junction and a certain shunt distribution with and without illumination is a non-trivial task,¹⁵ which is beyond the scope of this contribution. However, it is clear that, in regions of high series resistance and under load conditions, the local emitter potential will deviate from the potential applied to the contact leads. In the following sections, we will perform realistic simulations of this effect for a special geometry, both in the dark and under illumination. In regions of increased

contact resistance, these potential deviations are expected to be especially large, as will be shown below. In the Corescan method^{8,9} the emitter potential is directly measured with a mechanical probe, applying local illumination around the probe while short-circuiting the cell during the scan. It will be shown in the following that, under appropriate conditions, lock-in thermography results may also deliver information about the local emitter potential under load conditions.

2.1. R_s -imaging by dark lock-in thermography (R_s -DLIT)

Until now DLIT investigations have been performed mostly at a forward bias, close to the maximum power point, which is approximately 500 mV for typical Si cells. The dark current flowing under this condition (typically $< 2 \text{ mA/cm}^2$) is small against the short-circuit current (typically 30 mA/cm^2), so that series resistance effects are expected to be weak. Under this condition the depletion region recombination current and ohmic shunts dominate the dark I - V characteristic, hence this condition is optimal for imaging local shunts. It was recognized very early¹⁶ that, if DLIT is performed at a larger current density, the series resistance in the cell may lead to local Joule heating in the busbars and to an inhomogeneously distributed surface potential. Hence, for large currents the bias pulse excitation reduces with increasing distance to the current feed-in points, which disturbs the interpretation of the results. Therefore, for imaging shunts the high-current operation regime was hitherto deliberately avoided.

In the following, exactly this voltage drop effect will be exploited. Assuming no shunting in a certain region of interest, at a sufficiently large forward bias the local J - U characteristic can be described in good approximation as a pure diffusion current density:

$$J_{\text{diff}}(x, y) = J_0(x, y) \exp\left(\frac{e(U - \Delta U(x, y))}{kT}\right) \quad (8)$$

where $J_0(x, y)$ = local saturation current density, U = bias applied to the current leads. $\Delta U(x, y)$ is the voltage drop across the effective series resistance to the position (x, y) , which itself depends on $J_{\text{diff}}(x, y)$. Hence the local bias at the pn -junction is $U(x, y) = U - \Delta U(x, y)$. In an insufficiently contacted region suffering from a large series resistance, $U(x, y)$ will be considerably smaller than the applied bias U . This will be modelled in the following by assuming a 20-mm-diameter circular area of a non-contacted emitter (sheet resistance $\rho_s = 50 \text{ } \Omega/\text{square}$) surrounded by a circular emitter contact line providing a well-defined applied emitter potential U at a radius of $r = 10 \text{ mm}$. A constant saturation current density of $J_0 = 1.5 \times 10^{-12} \text{ A/cm}^2$ will be assumed, and any shunting (both linear and nonlinear) will be excluded. Then the lateral emitter current I_{lat} will be a radial one ($I_{\text{lat}} = 2\pi r J_{\text{lat}}$) and will be zero at the centre of the circular region. This system can be described by the following equations:

$$J_{\text{diff}}(r) = J_0 \exp\left(\frac{eU(r)}{kT}\right) \quad (9)$$

$$\frac{dI_{\text{lat}}(r)}{dr} = 2\pi r J_{\text{diff}}(r) \quad (10)$$

$$\frac{dU(r)}{dr} = \frac{\rho_s}{2\pi r} I_{\text{lat}}(r) \quad (11)$$

Equations (9–11) were solved numerically using MATHCAD¹⁷ for a boundary value of $I_{\text{lat}}(0) = 0$ and values of the applied potential $U_1(10 \text{ mm}) = 588 \text{ mV}$ and $U_2(10 \text{ mm}) = 606 \text{ mV}$, corresponding to a total injection current of 1 and 2 A for a 100 cm^2 sized cell without contact problems. The solutions are shown together with the resulting power dissipation profiles in Figure 2. The surface potential profiles in Figure 2(a) show the potential

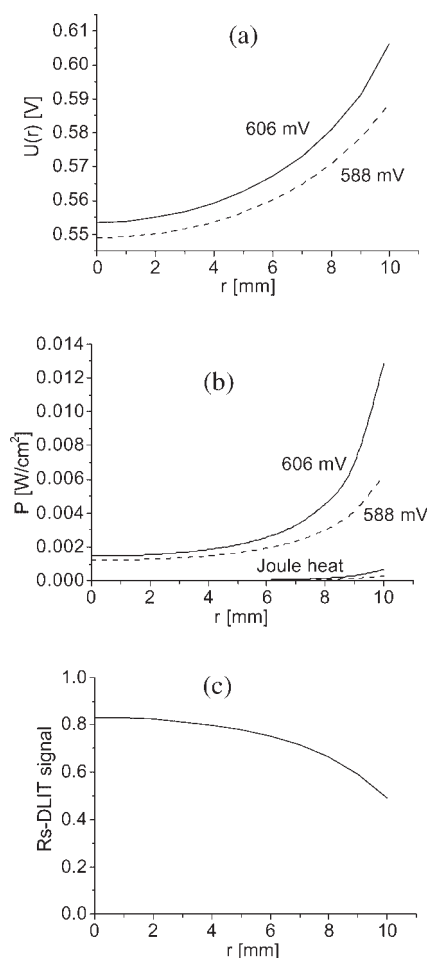


Figure 2. (a) Radial potential distribution; (b) dissipated power density (top of graph: total power, bottom: only Joule heat) for current flowing in the dark into a circular (10 mm radius) non-contacted region of a solar cell at two biases $U_1 = 558$ mV and $U_2 = 606$ mV applied at $r = 10$ mm; (c) Rs-DLIT signal: $P(U_1)/P(U_2)$

difference between the two applied voltages, which is about 18 mV at the edge of the non-contacted region and reduces to 4 mV at the centre of the region. The power density profiles in Figure 2(b) represent the sum of the injection heat (Equation 7), being the sum of Equation (2) and the diffusion part of Equation (4), the contact Peltier coolings (Equations 3 and 5), and the Joule heat (Equation 6). The local Joule heat contribution due to the lateral current flow in the emitter is shown separately at the bottom of the graph. It turns out that the Joule heat is small compared with the injection heat under these experimental conditions. Within the non-contacted region the dissipated power drops to 1/5th and 1/10th of the value in the contacted region ($r > 10$ mm) for U_1 and U_2 , respectively. Thus, if a DLIT experiment is performed using a sufficiently large forward bias so that a large current of the order of the short-circuit current is flowing, regions of unusually low signal may already indicate regions of a high series resistance, which may be caused, e.g., by an insufficient emitter contact resistance.

Unfortunately, especially in multicrystalline silicon solar cells, there may be large inhomogeneities of the local saturation current $J_0(x,y)$. Note that J_0 is proportional to the inverse of the minority-carrier lifetime, which may fluctuate by more than an order of magnitude across the area of a multicrystalline silicon solar cell. Therefore, without having any information about the lifetime distribution, it may be hard to distinguish

regions of high series resistance (showing a lower $U(x,y)$, see Figure 2a) from regions of high lifetime, where $J_0(x,y)$ is low. Here, we propose to correct for these inhomogeneities by using the local power ratio obtained from two dark lock-in thermograms taken at bias U_1 and U_2 . If both biases are so high that the diffusion current (Equation 8) dominates, and if the series resistance can be neglected ($\Delta U(x,y) = 0$), this ratio is:

$$R_s\text{-DLIT} = \frac{P_1}{P_2} = \frac{U_1 J_{\text{diff}}(U_1)}{U_2 J_{\text{diff}}(U_2)} = \frac{U_1}{U_2} \exp\left(\frac{eU_1 - eU_2}{kT}\right) \quad (12)$$

Following our suggestion in the introduction, we propose to name this dimensionless signal Rs-DLIT, since this is a special dark lock-in thermography signal, aiming to image regions of high series resistance. Hence, by using the ratio (Equation 12), at least in well-contacted regions the dependence on the local saturation current density should cancel and the result is dependent only on the applied biases. However, for $U_2 > U_1$ this ratio considerably increases in regions of high contact resistance, as the simulation in Figure 2(c) clearly shows. Optimum choices for U_1 and U_2 are forward biases for which the dark forward current is close to 1/3 and 2/3 of the short-circuit current of the device. If the biases are chosen lower, there is the danger to approach the regime where the depletion region recombination current dominates, for which Equation (12) no longer holds. If the biases are chosen too high, the series resistance of the metallization and emitter may be sufficient that Equation (12) is no longer valid. Note that for these high current experiments it is strongly recommended to increase the conductivity of the busbars of the cell, e.g., by metal stripes or by multiple contacting in order to avoid voltage drops along the length of the busbars.

2.2. R_s -imaging by illuminated lock-in thermography (R_s -ILIT)

It will be discussed in more detail in section 4 that one of the limitations of the Rs-DLIT technique proposed above is the low LIT signal strength in the non-contacted regions. Therefore, to obtain a sufficient signal-to-noise ratio in an acceptable measuring time, a high signal acquisition time or a low lock-in frequency has to be chosen for Rs-DLIT experiments. Another limitation is the influence of local shunts, which will be discussed in the following section. These limitations may be overcome by performing a recently introduced special type of lock-in thermography under illumination called Rs-ILIT.¹⁴ In the following an internal quantum efficiency of 1 is assumed, hence all photogenerated carriers are assumed to lead to a photocurrent I_{ph} . In solar cell research, the term ‘photocurrent’ is often used not for the short-circuit current, but for a current equivalent to the total rate of electron–hole pair generation. If white light is used for these experiments, a considerable fraction of the generated electrons does not contribute to the net photogenerated current, but recombines in the bulk or at the back contact. In this case our above assumption would be inaccurate, and an additional introduction of power sources regarding the thermalization and recombination of this fraction would be necessary. However, the assumption of an internal quantum efficiency of 1 is a good approximation for monochromatic illumination at $\nu = 880$ nm, as it will be assumed in the following modelling. Moreover, it will be shown below that for the Rs-ILIT technique with constant illumination to be introduced, this power contribution cancels by the lock-in process. Therefore, in this contribution we will use the term ‘photocurrent’ for the net photocurrent, still having in mind that for the correct interpretation of pulsed illumination LIT experiments in certain wavelength ranges, additional power sources might be necessary to describe the solar cell completely. It will also be assumed that the photocurrent is preferentially an electron current flowing from the base into the emitter, which is a good approximation as well, as long as 880 nm light is used for the experiments. First we will discuss which new heat sources appear if light is irradiated to the solar cell. It has already been discussed^{4–6} that there are two additional contributions: the thermalization heat P_{th} , which comes from the fact that the photon energy $h\nu$ is larger than the gap energy E_g , and the thermalization heat that is dissipated if photogenerated electrons are swept from the base through the pn -junction into the emitter. Note that the thermalization of photogenerated carriers flowing across the pn -junction is physically the inverse of the Peltier cooling P_{pn} for injection at the pn -junction (Equation 4) discussed in the previous section, but with the opposite sign. Therefore, it can also be called ‘Peltier heating’

and is another contribution to P_{pn} . Under illumination, for a photocurrent of I_{ph} the total amounts of the two additional power contributions are:

$$P_{th} = \frac{I_{ph}}{e} (h\nu - E_g) \quad (13)$$

$$P_{pn} = \frac{I_{ph}}{e} (E_g - \xi_n - \xi_p - eU) \quad (14)$$

Under illumination Equation (14) has to be added to Equation (4), and for the Peltier terms at the contacts (Equations 3 and 5) the difference between the diffusion current (Equation 8) and the photocurrent I_{ph} has to be used. Equations (9) and (11) remain valid under illumination, but Equation (10) changes to:

$$\frac{dI_{lat}(r)}{dr} = 2\pi r (J_{diff}(r) - J_{ph}) \quad (15)$$

Using these formulas, the modelling of the circular non-contacted region was also performed for the illuminated case, assuming a homogeneous photocurrent $J_{ph} = 30 \text{ mA/cm}^2$. Again, any shunting has been excluded in this calculation. The results of this modelling for several biases are shown in Figure 3. Since under illumination the current is laterally flowing out of the non-contacted area, the potential inside this area is larger than that outside this area. In the center of the non-contacted region, the potential is close to the open-circuit voltage, if the surrounding cell is at finite loads leading to 450 and 550 mV bias at the periphery of the non-contacted region. However, under short-circuit conditions at the periphery, the centre potential is below 400 mV. As mentioned above, for calculating the dissipated power profiles, a wavelength of the illuminating light of 880 nm and a quantum efficiency of 1 have been assumed. In the dissipated power density profiles (Figure 3b), the total dissipated power density is shown together with the different Joule heatings, that are again indicated at the bottom of the graph. At open-circuit and short-circuit the complete photon energy of 1.4 eV is dissipated for each absorbed photon in the cell, leading to a power density of 0.042 W/cm^2 . Above the maximum power point bias of the cell (which is about 550 mV here) the injection heating (Equation 7) plays an increasing role, therefore in this regime the power dissipated in the cell increases with increasing bias. This holds towards the centre of the non-contacted region, if the edge is kept at mpp-potential. Below the maximum power point bias, injection heating becomes negligible. On the other hand, the Peltier heating (Equation 14) increases with decreasing bias. This holds towards the centre of the non-contacted region, if the edge is at short-circuit. Hence, at the maximum power point the cell dissipates the smallest amount of thermal power.¹⁴ Compared with open-circuit or short-circuit conditions, it can also be that, at maximum power point, the cell is 'cooled' most by the power delivered to the load, as been pointed out already by Rappich et al.⁷ Joule heating again plays only a minor role here, but is largest under short-circuit conditions (as used by Isenberg et al.⁴ to image Joule heating in the emitter) and increases here towards the edge of the region at $r = 10 \text{ mm}$. This is the reason why, under short-circuit conditions the total dissipated power density exceeds the irradiation power density of 0.042 W/cm^2 towards the edge of the non-contacted region. However, the average dissipated power still equals the irradiation power density. Knowing these dependencies, the dissipated power profiles in Figure 3(b) can easily be understood. The decisive point is that under short-circuit conditions at the contacts, the potential of the non-contacted region is below that of the maximum power point. On the other hand, if the outer cell is at a finite load, leading to a bias close to the maximum power point there, the potential of the non-contacted part is already close to open-circuit potential. This is the reason why the power profiles cross. In the non-contacted region the dissipated power is larger under finite load than under short-circuit, but in the well-contacted region the opposite holds.

Just as for Rs-DLIT, it will be attempted now to find a combination of ILIT results which reacts most sensitively to inhomogeneities of the series resistance. According to the results shown in Figure 3(b) and discussed above, the difference between ILIT thermograms taken at finite load (close to the maximum power point) and under short-circuit seems to be most appropriate to detect regions of high series resistance.¹⁴ Indeed, as

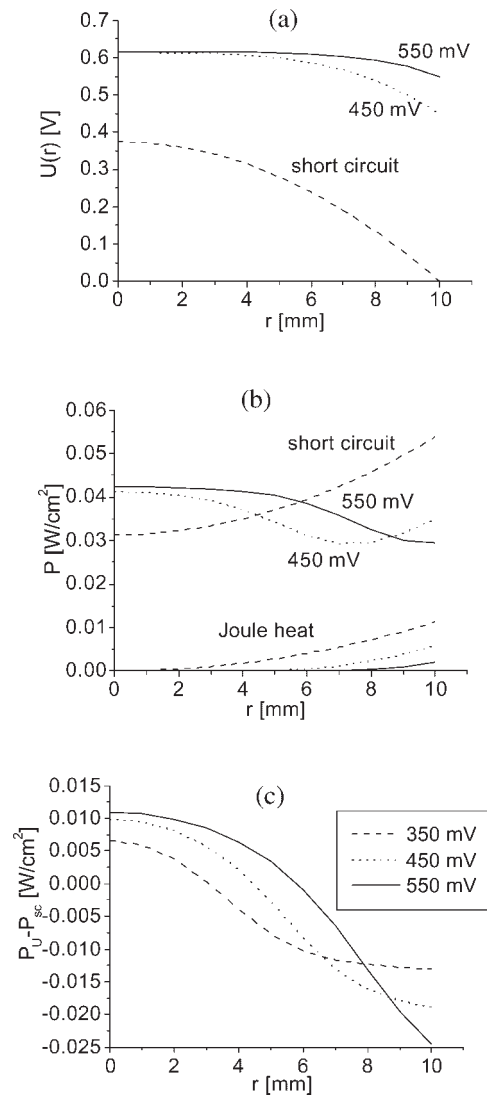


Figure 3. (a) Radial potential distribution; (b) dissipated power density (top of graph: total power, bottom: only Joule heat) for current flowing under illumination out of a circular non-contacted region of a solar cell for different biases; (c) Rs-ILIT signal ($P(U) - P_{sc}$) profiles for different biases

Figure 3(c) shows, this difference signal changes its polarity. In well-contacted regions it is negative because of the larger Peltier heating under short-circuit, but in non-contacted regions it is positive because there the injection heating (Equation 7) takes place only if the surrounding is at finite load conditions.

An easy way to obtain this difference image is to keep the illumination intensity constant and to change only the load of the cell periodically in the lock-in thermography (LIT) experiment. This can be done, e.g., by using an adjustable resistor and a relay, as proposed by Rappich *et al.*⁷ except that in our case the relay has to switch to short-circuit and not to open-circuit. Alternatively, if the power supply of the LIT system also has current-sinking capability, the bias can also be varied electronically from 0 V to a certain voltage, as can be done by using the Thermosensorik TDL 384 'M' Lock-in thermography system.¹⁸ If a constant light source is used in a LIT experiment, any thermalization loss (Equation 12) as well as any absorption of light outside the spectral sensitivity range of the solar cell automatically cancels by the lock-in process. Hence, for this purpose even a simple halogen lamp can be used, if the sample is appropriately cooled. The experimental results shown in

Section 3 are obtained in this way. Compared with performing separate capture of two pulsed light ILIT images under constant load, the proposed technique saves 50% of the measuring time and needs no further image processing. Note that, for this type of measurement, instead of the amplitude image the -90° image has to be displayed, since only this kind of representation allows to distinguish between positive and negative signal values. We propose¹⁴ to name this special technique Rs-ILIT, since this is a special ILIT technique aiming to image regions of high series resistance.

2.3. The influence of shunts

Until now, shunting has been neglected in our considerations. However, if there is any shunting current in the investigated solar cell, which may show either a linear or a nonlinear I - V characteristic, these shunts will become visible both in Rs-DLIT and in Rs-ILIT. In Rs-DLIT, if there are any current contributions deviating from Equation (8), even in the absence of series resistances Equation (12) no longer holds. In fact, in Rs-DLIT shunting regions appear bright, hence they may be misinterpreted as high-resistance regions. The only way to avoid this misinterpretation is to compare the Rs-DLIT image with an mpp-DLIT shunt image taken conventionally at, say, 500 mV forward bias close to the maximum power point. In this image all shunts are visible, but the diffusion current is not visible yet. If a structure is visible both in the DLIT shunt image and in the Rs-DLIT image, it has to be interpreted as a shunt, as demonstrated in the following section.

Also in Rs-ILIT shunts are producing a bright contrast, which may be misinterpreted as a region of high series resistance. However, here the influence of shunts can be corrected by subtracting the corresponding DLIT image taken under the same biasing conditions.¹⁴ Note that the biasing sequence of Rs-ILIT is identical to that of mpp-DLIT, except that constant light is irradiated. If there are any shunts present, which dissipate power at an applied bias, their signal should be the same with and without illumination. Thus, if the -90° DLIT image taken at the same pulsed bias is subtracted from the Rs-ILIT image, the latter should be corrected for shunt signals. The practical problem here is to find the correct biasing conditions for the DLIT measurement regarding all internal and external voltage drops, as well as the different internal bias distributions in the cell with and without illumination. It had been pointed out, e.g., by Isenberg and Warta⁴ that these distributions may differ, leading to different shunting currents under both conditions. We propose here to perform the DLIT image for correcting the Rs-ILIT image at a bias corresponding to a certain dark current. This dark current should be of the order of the difference between the short-circuit current and the current flowing at the bias used for the Rs-ILIT measurement. Nevertheless, this correction may be only an approximation, since the bias distribution in the cell is different with and without illumination. Moreover, because of the Peltier effect at the base contact P_{BM} (see Equation 5) the heat dissipated at a shunt may depend on whether the shunt current is flowing in the dark or is optically injected.⁶ Especially, if shunts occur in regions of large series resistance, their thermal signal will considerably differ between illuminated and non-illuminated conditions, even if the correct net current difference is used for the DLIT measurement. Also in this case only a qualitative distinction can be made. If bright regions in the Rs-ILIT image coincide with shunts, this contrast may be shunt-induced. Nevertheless, the shunt correction of the Rs-ILIT image may be very helpful, as the examples in the following section show. Altogether it has to be stressed that for distinguishing high-resistance regions from shunts, three separately measured LIT images are required for Rs-DLIT (two for calculating the actual Rs-DLIT image and one shunt image) and two images for Rs-ILIT (the actual Rs-ILIT image and one shunt image).

3. EXPERIMENTAL RESULTS

Previous ILIT experiments have been made with the solar cell freely lying on a thermostatted metal base, hence the IR camera and the illumination were both acting at the front side of the cell.⁴⁻⁶ This arrangement has the advantage that it is simple and the sample can easily be temperature controlled, but it has the disadvantage that the illumination has to be performed inclined to the cell, which may cause problems with the light intensity and homogeneity, if a LED array or a conventional lamp should be used for illumination. Moreover, in this configuration the cell is not allowed to be covered by a black IR emitter foil (which would prevent the illuminating

light reaching the sample), hence the IR emissivity is not homogeneous. In our ILIT sample holder the cell is sucked by vacuum between two thin plastic foils, one being transparent and the other blackened. The emitter of the cell faces through the transparent foil to the illuminating light, and the black foil covers the back surface of the cell, hence the IR images are taken from the back surface here. Note that the cell and its metallic back contact are sufficiently transparent to the thermal waves in the frequency range 3–30 Hz, belonging to a thermal diffusion length³ between 3 and 1 mm. The electric contacts are provided by flexible gilded copper stripes, which are covering the whole busbars and are pressed to them by the vacuum between the two foils. The advantage of this sample holder is that, due to the black foil, the IR emissivity is large and homogeneous here, and that illumination by a LED array can easily be performed from a short distance with good homogeneity. One disadvantage of this solution is, however, that it is difficult to control the temperature of the sample. Therefore, for performing power dissipating investigations such as Rs-DLIT or Rs-ILIT, the cell has to be cooled, which was done by air blown to the cell with a fan. In order to avoid disturbing excessive temperature fluctuations to be captured by the IR camera, the cell should be air cooled from the illuminated side and not from the IR camera side. This sample holder has been used for all ILIT and DLIT results in this contribution.

As mentioned above, the Rs-ILIT results shown here were obtained by illuminating the cell with a simple halogen lamp instead of the monochromatic light assumed in the simulations. It was discussed in Section 2.2. that, for this special procedure, panchromatic illumination should be equivalent to monochromatic one, since the additional absorption and thermalization losses are compensated by the lock-in procedure. The first results presented in Figures 4 and 5 are from a 156 cm² monocrystalline cell, where deliberately a lateral temperature gradient was used during firing of the contacts.¹⁹ In this cell, no lateral inhomogeneity of the lifetime is expected. All LIT measurements shown here have been taken at a lock-in frequency of 10 Hz using an acquisition time of 1 h to obtain a good signal-to-noise ratio. However, at least the high-current DLIT and the Rs-ILIT

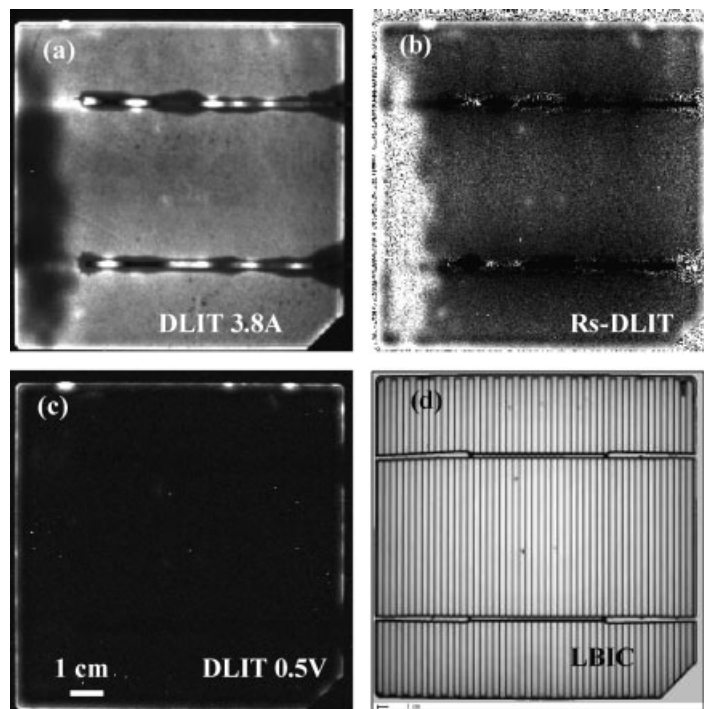


Figure 4. DLIT image taken at 3.8 A forward current: (a) (scaled from 0 to 4 mK), Rs-DLIT image based on images taken at 1.9 and 3.8 A; (b) (scaled from 0.4 to 0.7, dimensionless), DLIT image taken at 500 mV forward bias showing the shunt distribution, (c) (scaled from 0 to 1.5 mK) of a 125 × 125 mm² monocrystalline solar cell facing emitter contact problems; (d) LBIC image of the same cell showing the lifetime distribution

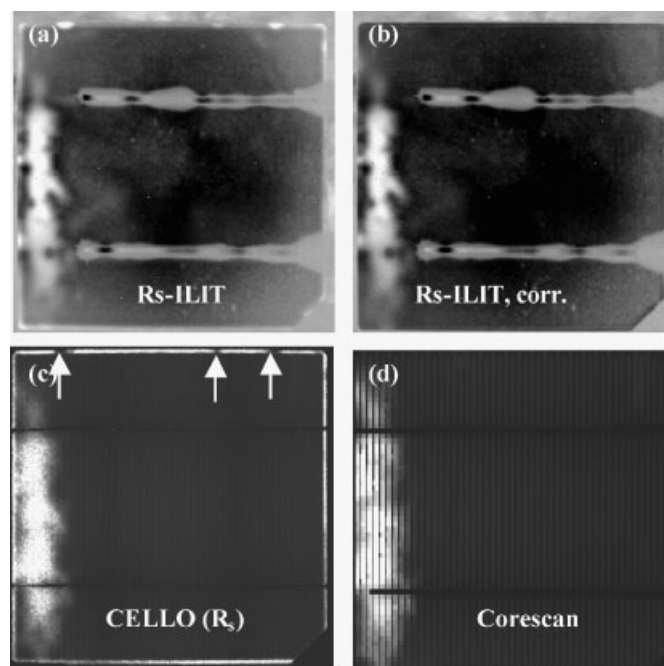


Figure 5. Rs-ILIT image (a) (uncorrected, scaled from -3 to 1 mK), shunt-corrected Rs-ILIT image; (b) (same scaling as a) CELLO R_s -image; (c) (arbitrary scaling; arrows: edge shunts) and Corescan image; (d) (arbitrary scaling) of the cell shown in Figure 4

images may be captured with an acceptable signal-to-noise ratio in 15 min. All scaling ranges are indicated in the captions. To enable a better comparison with the Corescan and CELLO images, all thermal images (which are taken from the back surface of the cell) are shown horizontally mirrored. Note that the contrast features visible in all LIT images the positions of the two horizontal busbars are due to two copper back contact leads, which have been used in these measurements for providing a low-ohmic contact to the cell. The DLIT image shown in Figure 4 (a) taken at 3.8 A forward current clearly shows a dark region at the left, which is most probably a region of high contact resistance. This is confirmed also in the Rs-DLIT image (Figure 4b, being the ratio of DLIT images measured at 1.9 and 3.8 A) showing a bright contrast in this region. Note that the noise level is considerably increased in the high-resistance region, as expected from our simulations. Figures 4(a and b) also show a bright signal and some bright spots along the edge, especially at the upper edge of the cell. As the DLIT image taken at 500 mV forward bias (Figure 4c) shows, this is an edge recombination current with local edge shunts. Note that in this image the high-resistance region is invisible. It is also not visible in the LBIC image (Figure 4d) taken under zero bias, which is always measured within the CELLO measurements. This LBIC image proves that there are no considerable lifetime variations in this cell.

Figure 5 shows results of the same cell taken under illumination. For our illumination conditions, which were below 1 sun, this cell showed a short circuit current of 4.26 A. The maximum power point was at 450 mV (measured at the current leads) at a current of 2.9 A. The correction DLIT image (not shown here) was measured at 580 mV, leading to a dark current of 1.3 A, which is just the current loss measured here at maximum power point. The uncorrected Rs-ILIT image in Figure 5(a) clearly shows the high-resistivity region with a much better signal-to-noise ratio than the Rs-DLIT image in Figure 4(b). As described before, Figure 5(a) is a LIT image taken under constant illumination with the bias pulsed between zero and the maximum power point, which is about 450 mV here (measured at the current leads). Also in this image the shunt-induced signals at the edges of the cell are present. In the shunt-corrected Rs-ILIT image Figure 5(b), however, the edge recombination signal and the shunts are no longer visible, which proves the effectiveness of the shunt correction procedure. The

somewhat higher signal level in the Rs-ILIT images towards the edges is due to an inevitable inhomogeneity of the illumination intensity in our setup. Figures 5(c and d) show the CELLO and Corescan images of this sample. Again, high-resistivity regions are displayed as bright contrast. The Corescan investigation has been performed after the thermal and the CELLO investigations, since these results are influenced by the weak scratches caused by the Corescan investigation. The correlation between CELLO and Corescan is excellent, and both images show a good correlation, both to the Rs-DLIT image (Figure 4b) and to the Rs-ILIT image (Figure 5b). Interestingly, the local edge shunts at the upper edge of the cell appear as dark contrast in the CELLO R_s image (see arrows in Figure 5c), they are not visible at all in the Corescan image (Figure 5d), and they appear as bright contrast in the Rs-DLIT image (Figure 4b) and in the uncorrected Rs-ILIT image (Figure 5b).

In Figures 6 and 7 results of a 100 cm^2 multicrystalline silicon solar cell are presented, which also shows regions of high emitter contact resistance. In this cell considerable inhomogeneities of the lifetime are expected. Figure 6 shows a DLIT image taken at 2 A forward current (a), an Rs-DLIT image using DLIT images obtained at 1 A and at 2 A forward current (b), a DLIT image measured at a forward bias of 0.5 V, showing the shunt distribution in this cell (c), and an LBIC image showing the lifetime distribution in this cell (d). Indeed, the 2 A DLIT image in Figure 6(a) shows a much stronger contrast than Figure 4(a), most of this contrast being due to an inhomogeneous lifetime distribution. The comparison shows that the 2 A DLIT-image (a) correlates to a certain degree with the lifetime distribution (d), as expected: Dark regions in (a) correspond to bright regions in (d) and vice versa. But this does not hold for all features in the DLIT images, for example not for the dark regions indicated by arrows in Figure 6(a). As Figure 6(c) shows, these regions are also no shunting sites, and in the Rs-DLIT image (Figure 6b) they appear bright as well (see arrows). Thus, these regions are clearly regions of unusually large series resistance. Apart from these regions there is only little correlation between the DLIT image (Figure 6a), which is essentially governed by the local distribution of the saturation current density J_0 , and the Rs-DLIT image (Figure 6b). This points to the fact that the J_0 correction made by Equation (12) was indeed

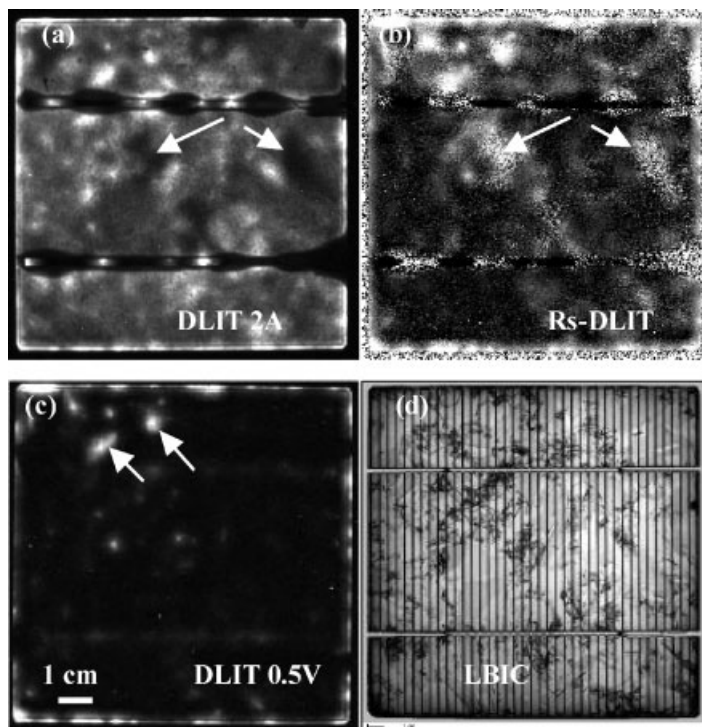


Figure 6. DLIT image taken at 2 A forward current (a) (scaled from 0 to 3 mK), Rs-DLIT image based on DLIT images taken at 1 and 2 A; (b) (scaled from 0.4 to 0.7, dimensionless), DLIT image taken at 500 mV forward bias showing the shunt distribution; (c) (scaled from 0 to 0.5 mK) of a $100 \times 100\text{ mm}^2$ cast multicrystalline silicon solar cell facing emitter contact problems; (d) (arbitrary scaling) LBIC image of the same cell showing the lifetime distribution

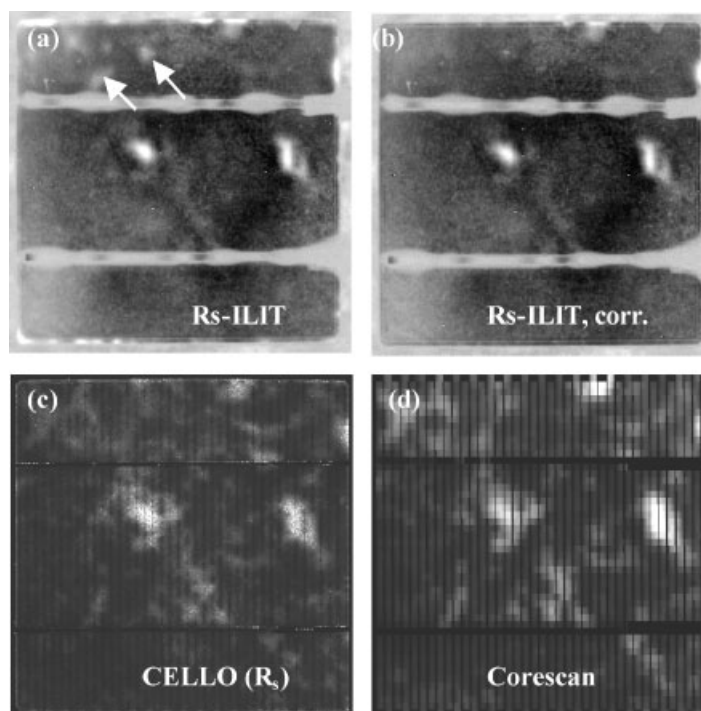


Figure 7. Rs-ILIT image (a) (uncorrected, scaled from -3 to $+0.5$ mK), shunt-corrected Rs-ILIT image; (b) (same scaling as a) CELLO R_s -image; (c) (arbitrary scaling); and (d) Corescan image (arbitrary scaling) of the cell shown in Figure 6

effective. Note that, e.g., the regions indicated by arrows in the shunt image (Figure 6c) coincide with bright regions in the Rs-DLIT image (Figure 6b). This indicates that these regions may be shunts. The same holds for the signal at the circumference of the cell, which is caused by nonlinear edge shunts.

Figure 7 summarizes images taken with the multicrystalline cell of Figure 6 under illumination. In Figure 7(a) the uncorrected Rs-ILIT image is shown, which is a -90° image measured under constant illumination with the bias of the cell pulsed between 0 mV (short-circuit) and the maximum power point of 460 mV (both values measured at the current leads). Under short-circuit the measured cell current was about 2.68 A (the illumination intensity was below 1 sun), and under 460 mV it was about 2.35 A. Also here, the somewhat increased signal value towards the edges of the cell is due to an inhomogeneous illumination intensity. There is a good correlation between the Rs-DLIT and the Rs-ILIT image with the Rs-ILIT image, again showing a considerably better signal-to-noise ratio. For performing the shunt correction, a -90° DLIT image measured at 540 mV, leading to a dark current of 0.3 A, has been used, which is roughly the difference between the short-circuit current and that at the maximum power point. In the shunt-corrected Rs-ILIT image (Figure 7b) the signal of the shunts indicated in Figure 6(d) as well as most of the bright regions at the circumference of the cell have disappeared. This indicates that these features have been caused by shunting and that the shunt correction procedure also works correctly in this case. The comparison with the two independent series resistance imaging techniques CELLO and Corescan (performed after the other investigations) also shows a good correlation in this case. Hence, the dominant high series resistance regions can be imaged reliably by all these different techniques also for the inhomogeneous distribution of the minority carrier lifetime that is found in multicrystalline silicon solar cells.

4. DISCUSSION AND OUTLOOK

It has been shown that, under appropriate experimental conditions, lock-in thermography (LIT) delivers not only information about shunting sites and local recombination sites, but also about regions of high series

resistance. Especially if the informations of two LIT images are properly combined, the influence of other inhomogeneities in the cell (e.g., of the lifetime) can be eliminated. It has been shown that this is especially necessary in multicrystalline cells that usually have a considerable lateral inhomogeneity of the lifetime. Based on the local electrothermal modelling of a non-contacted region in a solar cell, two new LIT imaging modes called Rs-DLIT and Rs-ILIT are proposed, and first experimental results are introduced. These results are compared with Corescan and CELLO results of the same samples, which are known to provide reliable information about the local series resistance. Though the comparison of all these techniques delivers consistent results, some limitations of the new thermographic techniques have to be mentioned. One major limitation of Rs-DLIT is its low signal strength in non-contacted regions. As our simulations (Figure 2b) have shown, inside a non-contacted region the dissipated power density may be reduced to 1/5th to 1/10th of the value in a well-contacted region. In this respect the Rs-ILIT technique behaves better by a factor of 10, as Figure 3(c) compared with Figure 2(b) shows. Hence, one advantage of Rs-ILIT compared to Rs-DLIT is that it needs a lower signal acquisition time. While for the two DLIT measurements needed for Rs-DLIT at a lock-in frequency of 10 Hz a measuring time of more than 1 h is necessary, the (single) Rs-ILIT measurement can be performed within 0.25 h for a comparable signal-to-noise ratio. One limitation of both techniques is that local shunts are producing a signal that is similar to that of regions of high series resistance. In order to avoid any misinterpretation, Rs-DLIT and Rs-ILIT results always should be compared with DLIT shunt images measured at about 500 mV forward bias. In this respect, the second advantage of Rs-ILIT compared to Rs-DLIT is that only here the influence of shunts can be corrected by subtracting an appropriately measured DLIT thermogram. This additional measurement needs roughly the same acquisition time than the Rs-ILIT one, but both together are still shorter than a comparable Rs-DLIT measurement. Thus, it can be concluded that Rs-ILIT is more reliable for detecting series resistance inhomogeneities and also more sensitive than Rs-DLIT. On the other hand, Rs-ILIT is experimentally more demanding than Rs-DLIT, since it needs an appropriate light source delivering a homogeneous illumination and an appropriate sample holder. However, in contrast to conventional ILIT investigations,^{4,5} this illumination does not need to be pulsed and may even be panchromatic.

Note that the signal generation mechanism for Rs-DLIT and Rs-ILIT is highly nonlinear. Therefore, these signals can hardly be interpreted quantitatively in terms of a well-defined series resistance to a certain position in the solar cell, which is possible both for Corescan^{8,9} and for CELLO.^{10,11} It has to be admitted that Corescan provides a better signal-to-noise ratio and is not as strongly affected by local shunting as the thermal techniques introduced here, but it is not strictly non-destructive. On the other hand, CELLO provides a better spatial resolution and also a better signal-to-noise ratio than Rs-DLIT and Rs-ILIT, but its signal is also influenced to a certain degree by local shunts. Moreover, CELLO is only beginning to become commercialized, and it needs a measuring time of several hours per cell for high spatial resolution. Thus, the new thermal techniques introduced here have the main advantage that they are strictly non-destructive and show a reasonable measurement speed. Together with the hitherto established lock-in thermography techniques¹⁻⁶ they allow one to perform a comprehensive analysis of all local energy loss mechanisms in solar cells, including shunting below grid lines, which is accessible neither by CELLO nor by Corescan.

In this contribution, a complete local electrothermal simulation of a defect in a solar cell (circular non-contacted region) with and without illumination was performed. Similar simulations can be very helpful to interpret, e.g., oc-ILIT results obtained on recombinative defects like grain boundaries.^{4,5} In these simulations also lateral inhomogeneities of the photocurrent and of the saturation current density should be included, which in the present simulation have both been assumed to be homogeneous. Also recombination heat dissipated at local defects, both in the depletion region and in the bulk or at the back surface, and the different depths of different heat sources below the surface of the cell, should be explicitly included, which has not been regarded here.

Acknowledgements

This work was supported by the German BMBF under contract 0329846 D (ASIS). We wish to thank J. Isenberg and W. Warta (ISE Freiburg) and M. Kaes and G. Hahn (University of Konstanz) for stimulating discussions.

REFERENCES

1. Breitenstein O, Langenkamp M, Lang O, Schirmmayer A. Shunts due to laser scribing of solar cells evaluated by highly sensitive lock-in thermography. *Solar Energy Materials and Solar Cells* 2001; **65**: 55–62.
2. Breitenstein O, Langenkamp M, Rakotoniaina JP, Zettner J. The imaging of shunts in solar cells by infrared lock-in thermography. *Proceedings of the 17th European Photovoltaic Solar Energy Conference*, Munich, 2001; 1499–1502.
3. Breitenstein O, Langenkamp M. *Lock-in Thermography—Basics and Use for Functional Diagnostics of Electronic Components*. Springer: Berlin, 2003.
4. Isenberg J, Warta W. Realistic evaluation of power losses in solar cells using thermographic methods. *Journal of Applied Physics* 2004; **95**: 5200–5209.
5. Isenberg J, Warta W. Spatially resolved evaluation of power losses in industrial solar cells by lock-in thermography. *Progress in Photovoltaics: Research and Applications* 2004; **12**: 339–353.
6. Kaes M, Seren S, Pernau T, Hahn G. Light-modulated lock-in thermography for photosensitive *pn*-structures and solar cells. *Progress in Photovoltaics: Research and Applications* 2004; **12**: 355–363.
7. Rappich J, Mueller M, Schneider F, Tributsch H. Thermographic sampling technique applied to microelectronics and photovoltaic devices. *Solar Energy Materials and Solar Cells* 1998; **53**: 205–215.
8. van der Heide ASH, Schönecker A, Wyers GP, Sinke WC. Mapping of contact resistance and locating shunts on solar cells using resistance analysis by mapping of potential (RAMP) techniques. *Proceedings of the 16th European Photovoltaic Solar Energy Conference*, Glasgow, 2000; 1438–1442.
9. van der Heide ASH, Bultman JH, Hoornstra J, Schönecker A. Error diagnosis and optimisation of c-Si solar cell processing using contact resistances determined with the Corescanner. *Solar Energy Materials and Solar Cells* 2002; **74**: 43–50.
10. Carstensen J, Popkirov G, Bahr J, Föll H. CELLO: an advanced LBIC measurement technique for solar cell local characterization. *Solar Energy Materials and Solar Cells* 2003; **76**: 599–611.
11. Carstensen J, Popkirov G, Bahr J, Föll H. In *Photovoltaic and Photoactive Materials—Properties, Technology and Applications*, Marshall JM, Dimova-Malinovska D (eds). Kluwer: Netherlands, 2002; 321.
12. van der Heide ASH. Apparatus for localizing production errors in a photovoltaic element. US Patent number US 6,750,662.
13. <http://www.sunlab.nl>
14. Breitenstein O, Rakotoniaina JP. Electro-thermal simulation of a defect in a solar cell. *Journal of Applied Physics* 2005; **97**: 074905.
15. Dicker J, Isenberg J, Warta W. Effect of shunt distribution on the overall solar cell performance investigated by circuit simulation. *Proceedings of the 17th European Photovoltaic Solar Energy Conference*, Munich, 2001; 1567–1570.
16. Breitenstein O, Eberhardt W, Iwig K. Imaging the local forward current density of solar cells by dynamical precision contact thermography. *Proceedings of the 1st World Conference on Photovoltaic Energy Conversion*, Hawaii, 1994; 1633–1636.
17. www.mathcad.com
18. www.thermosensorik.de
19. Hoornstra J, van der Heide ASH, Weeber AW, Granek F. New approach for firing optimisation in crystalline silicon cell technology. *Proceedings of the 19th European Photovoltaic Solar Energy Conference*, Paris, 7–11 June 2004; 1044–1047.